Accepted Manuscript

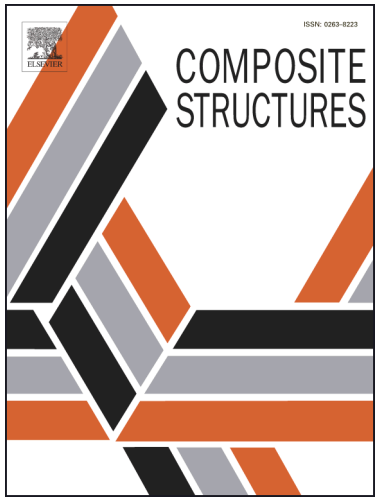

Development of composite springs using 4D printing method

Suong Van Hoa

PII: S0263-8223(18)31347-3
DOI: https://doi.org/10.1016/j.compstruct.2018.12.003
Reference: COST 10465

To appear in: *Composite Structures*

Received Date: 11 April 2018
Revised Date: 23 July 2018
Accepted Date: 4 December 2018

Please cite this article as: Van Hoa, S., Development of composite springs using 4D printing method, *Composite Structures* (2018), doi: https://doi.org/10.1016/j.compstruct.2018.12.003

Development of composite springs using 4D printing method

Suong Van Hoa
Concordia Center for Composites
Department of Mechanical, Industrial and Aerospace Engineering
Concordia University
Center for Research in Polymers and Composites (CREPEC)
Montreal, Quebec, Canada
hoasuon@alcor.concordia.ca

Abstract:

Composite springs have been used in many engineering applications, particularly in the transportation industry. This is due to their light weight, good stiffness, good strength, good corrosion and fatigue resistances. Normally special molds need to be prepared in the manufacturing of these springs. The molds have curvatures which fit into the shape of the final product.

Recently the concept of 4D printing of composites was introduced. This concept is a combination of 3D printing together with the reconfiguration of the part upon the activation of some mechanism such as heat, light, or the absorption of moisture. This concept allows the ability to make structures of complex shapes without the need to have complex molds. Layers of composites can be laid on a flat mold. Upon curing, the layers reconfigure into curved structures. As such, curved composite structures can be made using only flat molds. The mechanism for this reconfiguration depends on the anisotropic nature of layered composite materials.

This paper presents the fundamental study, as part of a larger project intended to use the concept of 4D printing to develop complex composite structures without the need for complex curved molds. The fundamental study examines the mechanical characteristics of curved composite beams made by 4D printing.

Introduction:

Relevant aspects of leaf springs.

Composite springs are used in many applications. Two typical applications are in leaf springs for automobiles (figure 1a) and in prostheses (figure 1b).

Conventional leaf springs are usually made of steel. They consist of either a single leaf or many leaves connected together. Composite leaf springs were introduced by General Motors as an option for conventional leaf springs in 1981. These composite springs consist mainly of curved composite laminates. The basic constituent of a composite leaf spring is a curved composite beam. The reason for the selection of composite springs is due to the light weight, high stiffness and good fatigue and corrosion resistances of composites [3]. Beardmore [4] studied the application of composite springs in automobiles. Morris concentrated on the use of composites for the rear suspension system [5]. Daugherty [6] studied the application of composite leaf

springs in heavy trucks. Yu and Kim [7] designed and optimized a double tapered beam for automotive suspension leaf spring.

Figure 1a: Examples of leaf springs [1]

Figure 1b: Example of prostheses [2]

The process of manufacturing composite leaf springs is usually Resin Transfer Molding (RTM). The process requires a high precision matched metal mold. Composite preforms are placed snugly inside the mold. Resin is then infused into the dry composite preforms using high pressure. Fibers are usually glass or carbon, and the matrix is usually epoxy.

Typical dimensions of composite leaf springs are shown in Table 1.

Table 1: Typical dimensions of composite leaf springs for automotive applications

Items	Typical dimensions
Total length (mm)	1000
Width (mm)	50
Arc height (mm)	188
Radius of curvature (mm)	950
Thickness of leaf (mm)	10
Spring constant (N/cm)	400

Besides springs for automotive applications, composite springs have also been used for prostheses [2]. The manufacturing of these prostheses usually need to have a mold with curved configuration similar to that of the final part.

The concept of 4D printing

4D printing is a combination of 3D printing together with the reconfiguration of the simple shaped structure into complex shaped structures. First layers of materials with special properties are deposited using a method similar to 3D printing. Then the structure is subjected to the application of some activation mechanism such as heat, light, or the absorption of liquid such as water. This activation changes the configuration of the structure into some complex shape, depending on the design. 4D printing began with Tibbits [8]. A recent review is given in [9]. Most of the work on regular 4D printing utilizes materials that are soft and do not have high strength or stiffness. These materials are usually different types of plastics. Also in the regular 4D printing process, usually isotropic materials are used and different types of materials may be deposited at different locations within the same plane. The difference in the deformation behavior of materials at different locations within the plane give rise to the 3D shape change. The calculations for the deformed shape usually depends on the difference in deformation behavior of materials within one plane. As such the deformation is due to the difference in the characteristics of the materials at different locations, rather than due to the anisotropy of the materials, as in the case of 4D printing of composites, presented below.

The 4D printing of composites utilizes the concept of regular 4D printing. However 4D printing of composites uses materials made of long fiber embedded in polymeric resins. These are the long continuous fiber reinforced composites that have been used for many years to make airplanes, and automobiles etc. As such the materials used in 4D printing of composites have good strength, good stiffness, high fatigue resistance, and they are commercially available. The method of automated composites manufacturing is used to deposit many flat layers of composites to make stacks. The individual layers have different fiber orientations. Upon curing (application of heat), the resin cures, and serves as shear load transfer medium between the fibers. Upon cooling from the cure temperature down to room temperature, the difference in coefficients of thermal contraction between the different layers will provide the reconfiguration of the shape of the structure. Laminate theory can be used to determine and predict the curvatures created by the reconfiguration [10].

Requirements for 4D printing of composite springs

Radius requirement: The concept of 4D printing of composites can provide structures of complex shapes using only flat molds. For leaf spring applications, Table 1 shows that the curvature of the common springs is about 950 mm. The springs also only have cylindrical curvature. As such, only lay ups containing 0^o and 90^o fiber orientation need to be considered.

Table 2: Properties of composite materials [11]

Properties	Carbon/epoxy
E_1 (GPa)	155.0
E_2 (GPa)	12.1
G_{12}(GPa)	4.4
ν_{12}	0.248
α_1 (10^{-6}/C)	-0.018
α_2 (10^{-6}/C)	24.3
Longitudinal tensile strength (MPa)	1500
Longitudinal compression strength (MPa)	1250
Transverse tensile strength (MPa)	50
Transverse compressive strength (MPa)	200
Shear strength (MPa)	100

Using the properties of carbon/epoxy as shown in Table 2, with the assumption of thickness of each layer to be 0.125 mm, and laminate theory in [10], the radii of curvature for different laminates with different stacking sequences can be calculated and are shown in Table 3.

Experimental values:

A few laminates were made using carbon/epoxy materials (CYTEC 977-2). The layers were laid on a flat mandrel using an automated fiber placement machine, with a curing temperature of 177 ^oC [10]. After being taken from the autoclave, the radii of the laminates were measured and are shown in Table 3.

There is some difference between the calculated radii and the experimental radii. The reason for this can be due to the uncertainty in the contribution of the chemical shrinkage of the resin during the curing process. The chemical shrinkage tends to reduce the effect of the contraction coefficients and tend to result into larger radii of curvature.

Discussion:

Two main groups of laminates have been considered, namely the $[0/90_n]$ laminates and the $[0_2/90_n]$ laminates. These were examined to study the effect of adding more layers of 90^o on the radii of curvature. Figure 2 shows the variation of the curvature with respect to the value of *n*.

It can be seen that for the $[0/90_n]$ laminates, as *n* goes from 1 to 2, there is a reduction in the radius of curvature. After that, as *n* increases, the radius of curvature increases. For the group of laminates $[0_2/90_n]$, as *n* goes from 1 to 2 to 3, the radius of curvature decreases. After that, as *n* increases, the radius of curvature increases. This behavior is due to the shifting of the neutral axis toward the 90^o layers as the number of these layers increases.

Note that the radius of curvature of laminate $[0_2/90_2)$ is twice that of laminate [0/90]. In fact, it can be stated that the radius of curvature of a laminate in proportional to the thickness of the sub-laminate within the laminate. For example, the radius of curvature of laminate $[0_{16}/90_{24}]$ is twice that of the laminate $[0_8/90_{12}]$, and eight times that of the laminate $[0_2/90_3]$.

From figure 2, it can be seen that the $[0_2/90_n]$ laminates have larger radii of curvature than the $[0/90_n]$ laminate at small *n*, but as *n* increases, the curvatures of the two types of laminates approach each other.

In addition, a few thicker laminates were also examined. These were added in order to achieve similar properties with the current leaf springs as shown in Table 1. Among the different laminates, the one with $[0_{16}/90_{24}]$ lay up sequence has a radius of curvature of 93 cm, which is closest to the value of 95 cm shown in Table 1 for current composite springs. As such, this lay up sequence will be selected for experimental evaluation.

Table 3: Radii of curvatures, and included angles for laminates with different stacking sequences

Laminate	# layers	Thickness (mm)	Radius of curvature R (cm)	Radius of curvature (exp) (cm)	Included angle $2\theta_o$ radian(^{o}) (G=30.48 cm)
0/90	2	0.250	6.3	5.6-7.2.	4.87(279)
$0/90_2$	3	0.375	6.1	5.6-6.2	5.00(286)
$0/90_3$	4	0.500	7.6	6.3-7.0	4.01(230)
$0/90_4$	5	0.625	9.5		3.22(184)
$0/90_5$	6	0.750	11.5		2.65(152)
$0/90_6$	7	0.875	13.7		2.22(127)
$0/90_7$	8	1.000	15.9	14.6-15.9	1.92(110)
$0/90_8$	9	1.125	18.4		1.66(95)
$0/90_9$	10	1.250	20.8		1.47(84)
$0/90_{10}$	11	1.375	23.4		1.30(75)
$0_2/90$	3	0.375	20.1		1.52(87)
$0_2/90_2$	4	0.500	12.5	13.3	2.43(139)

$0_2/90_3$	5	0.625	11.6	13.8	2.63(151)
$0_2/90_4$	6	0.750	12.3		2.48(142)
$0_2/90_5$	7	0.875	13.6		2.25(129)
$0_2/90_6$	8	1.000	15.2		2.01(115)
$0_2/90_7$	9	1.125	17.0		1.79(103)
$0_2/90_8$	10	1.250	18.9		1.61(92)
$0_2/90_9$	11	1.375	21.0		1.45(83)
$0_2/90_{10}$	12	1.500	23.1		1.32(76)
$0_8/90_{12}$	20	2.500	46.4	60	0.65(38)
$0_{16}/90_{24}$	40	5.000	93	105	0.33(19)
$0_{24}/90_{36}$	60	7.500	139		0.22(13)

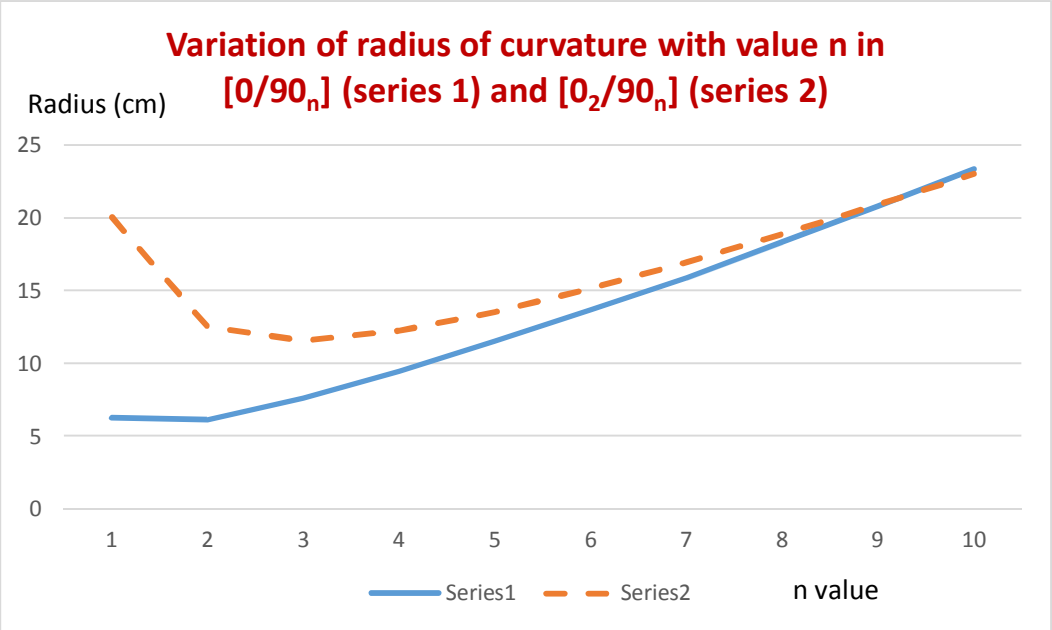

Figure 2: Variation of radii of curvature with respect to the value of *n* (calculated values).

Stiffness requirement

The stiffness of the curved beam depends on three elements. One is section modulus, which depends on the thickness and composition of the layers. The section modulus can be represented by the equivalent bending stiffness <EI>. The second element is the radius of curvature, and the third element is the length of the beam.

Bending section modulus:

The calculation of <EI> follows the sum of the contributions from the different layers and their positions in the stacking sequence. The bending section modulus of the laminate $[0/90_4]$ is shown below. The center of the coordinate axis z is taken to be the mid plane of the laminate:

$$< EI >= \frac{1}{12} b(3h)^3 E_{90} + \frac{1}{12} bh^3 E_{90} + bh(2h)^2 E_{90} + \frac{1}{12} bh^3 E_o + bh(2h)^2 E_o \quad (1)$$

Where <EI> represents the equivalent bending stiffness of the section.

b: is the width of the beam

h: is the thickness of each layer

E_{90} is the modulus of the 90° layer

E_o is the modulus of the 0° layer.

Collecting terms, equation (1) gives:

$$< EI >= \frac{bh^3}{12}(76E_{90} + 49E_o) \quad (2)$$

From table 2, the ratio for E_2/E_1 is (12.1GPa/155 GPa = 0.078). Using this value in equation (2) gives:

$$< EI >= \frac{E_o bh^3}{12}(54.9) \quad (3)$$

Following the same procedure, the expression for other types of laminates can be obtained.

For laminates of type $[0/90_n]$:

$$< EI >= \frac{bh^3}{12} E_{90}(n^3 + 3n) + \frac{bh^3}{12} E_o(1 + 3n^2) \quad (4)$$

For laminates of type $[0_2/90_n]$:

$$< EI >= \frac{bh^3}{12} E_{90}(n^3 + 12n) + \frac{bh^3}{12} E_o(8 + 6n^2) \quad (5)$$

Table 4: Stiffness and spring constant for different laminates ($E_o bh^3/12 = 1.92 \times 10^{-3}$ Nm^2)

Laminate	# layers	R (cm)	Normalized <EI>: <EI>/($E_o bh^3/12$)	Half included angle θ_o(rad)	Spring constant (N/cm) (12" or 30.48 cm long sample)	Spring constant (exp) (N/cm)
0/90	2	6.3	4.3	2.44		
$0/90_2$	3	6.1	14.1	2.50		
$0/90_3$	4	7.6	30.8	2.01		
$0/90_4$	5	9.5	54.9	1.61		

$0/90_5$	6	11.5	86.9	1.33	2.2	
$0/90_6$	7	13.7	127.3	1.11	2.8	
$0/90_7$	8	15.9	176.3	0.96	3.6	5.0
$0/90_8$	9	18.4	234.8	0.88	3.9	
$0/90_9$	10	20.8	303	0.74	5.4	
$0/90_{10}$	11	23.4	381.3	0.65	6.9	
$0_2/90$	3	20.1	15.0	0.76	2.8	
$0_2/90_2$	4	12.5	34.5	1.22	4.2	
$0_2/90_3$	5	11.6	66.9	1.32	4.9	
$0_2/90_4$	6	12.3	112.7	1.24	4.3	
$0_2/90_5$	7	13.6	172.4	1.13	3.8	
$0_2/90_6$	8	15.2	246.5	1.01	5.0	
$0_2/90_7$	9	17.0	335.3	0.90	6.5	
$0_2/90_8$	10	18.9	439.4	0.80	8.5	
$0_2/90_9$	11	21.0	559.2	0.73	10.2	
$0_2/90_{10}$	12	23.1	695.4	0.66	12.6	11.0
$0_8/90_{12}$	20	46.4	4282.5	0.33	71.7	
$0_{16}/90_{24}$	40	93	34253	0.17	509	486
$0_{16}/90_{24}$ (60.96cm long)	40	93	34253	0.34	64.6	60
$0_{24}/90_{36}$	60	139	115603	0.11	1838	

Values for <*EI*> for different laminates were calculated and shown in Table 4. Figure 3 shows the variation of the section modulus for laminates with different stacking sequences. It can be seen that as *n* increases, the laminate $[0_2/90_n]$ has faster increasing bending modulus than the $[0/90_n]$ laminates. It can also be seen that a laminate with stacking sequence $[0_{\alpha\, m}/90_{\alpha\, n}]$ would have the bending modulus <*EI*> that is α^3 times the bending modulus of laminate with stacking sequence $[0_m/90_n]$. For example, the laminate with stacking sequence $[0_{16}/90_{24}]$ has <*EI*> that is 8^3 (or 512) times the <*EI*> of laminate $[0_2/90_3]$.

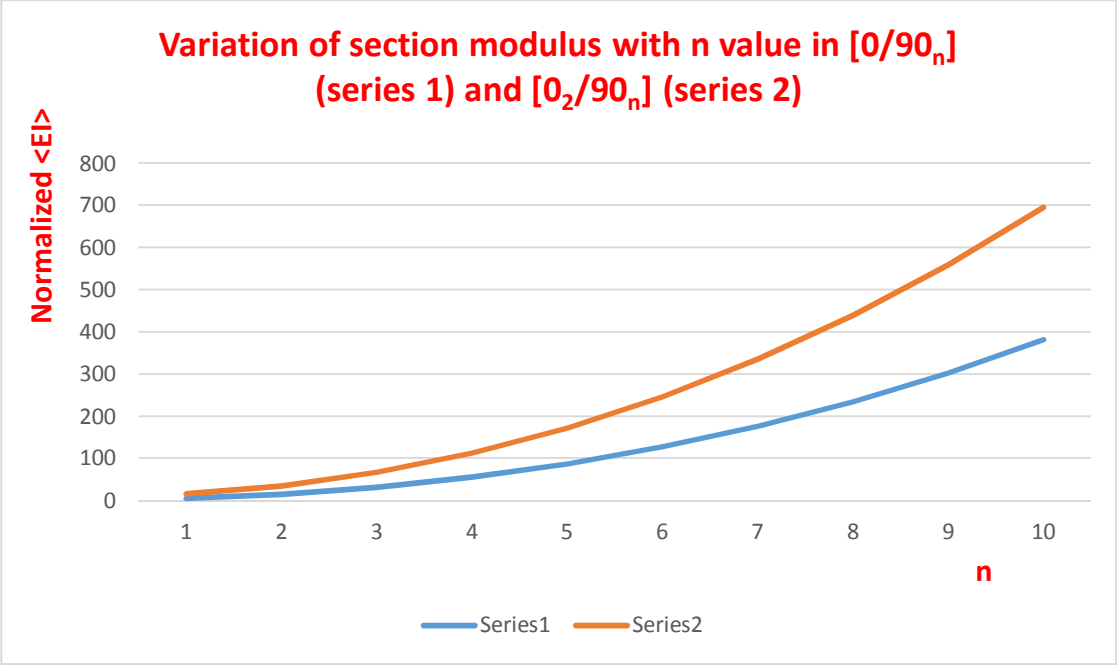

Figure 3: Effect of values of *n* on bending section modulus (lower curve-series 1, upper curve-series 2).

Effect of length and radius of curvature on bending stiffness:

The bending stiffness of the beam depends not only on the section modulus <*EI*> but also on the length and radius of curvature of the beam. Figure 4 shows the comparison between three configurations, where beams of the same lengths but different radii of curvature are shown. For the purpose of comparison, assuming that all beams have the same length G (different spans L), the same load P, and the same boundary conditions. For the case of curved beams, there is a relation between the radius R, the length G, the height d (figure 5), and the included angle θ_o.

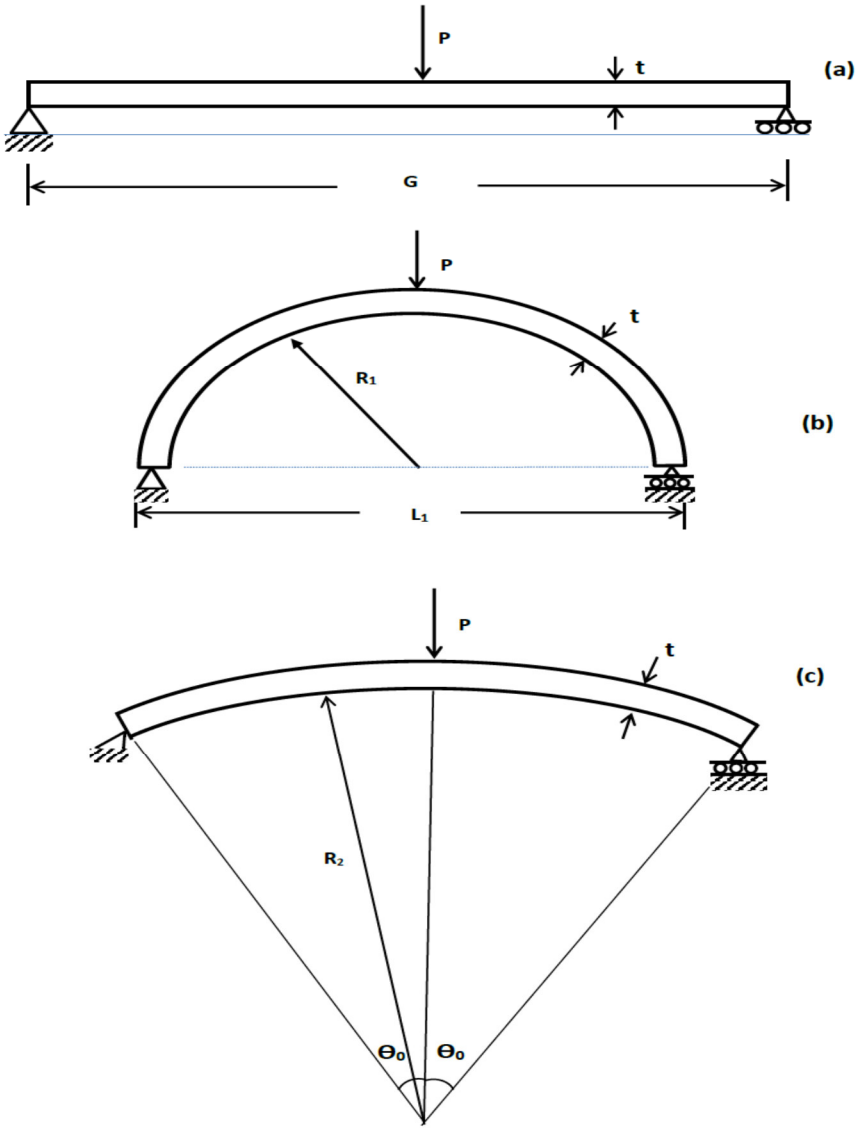

Figure 4: Comparison between three configurations

The lay up sequence will determine the radius of curvature R. The combination of G and R can be used to determine the span length L, the included angle $2\theta_o$, and the height d, via the following relations:

$$\theta_o = \frac{G}{2R} \tag{6}$$

Values for the included angle ($2\theta_o$) are calculated for spring of 12 inch (30.48 cm) long and are shown in Table 3.

The span L is given as:

$$L = 2R\sin\theta_o \tag{7}$$

And for the height d

$$d = R(1-\cos\theta_o) \tag{8}$$

Figure 4a shows the situation of a straight beam with span L = G, subjected to simply supported boundary conditions, and mid point loading. The displacement at mid length due to the load P is given as (assume isotropic material):

$$\delta_1 = \frac{PG^3}{48EI} \tag{9}$$

Figure 4b shows the situation of a curved beam (half circle with radius R) with the same length G, but with different span L_1, also subjected to a mid length load P. Figure 4c shows the situation of a curved beam with larger radius than the case 4b. It is of interest to determine the load/deflection relations for the cases 4b and 4c.

Figure 5 shows the parameters for analysis for the case of 4b and 4c (note that 4b is a special case of 4c). In this figure, all reactions at the support points are shown. In the case of simply supported beams, $M_A = M_B = H_A = 0$.

Let *s* be the coordinate along the length of the beam, the moment curvature relation can be written as:

$$\frac{d^2r}{ds^2} = \frac{M}{EI} \tag{10}$$

where r is the radial displacement of the beam.

This can be shown to be:

$$\frac{d^2r}{d\theta^2} = \frac{R^2\left[V_A R[\sin\theta_o - \sin(\theta_o - \theta)]\right]}{EI} \tag{11}$$

Where V_A is the reaction at the left end boundary. By equilibrium, it can be shown that $V_A = P/2$.

Integrating gives:

$$\frac{dr}{d\theta} = \frac{PR^3\left[\theta\sin\theta_o - \cos(\theta_o - \theta)\right]}{2EI} + C_1 \tag{12}$$

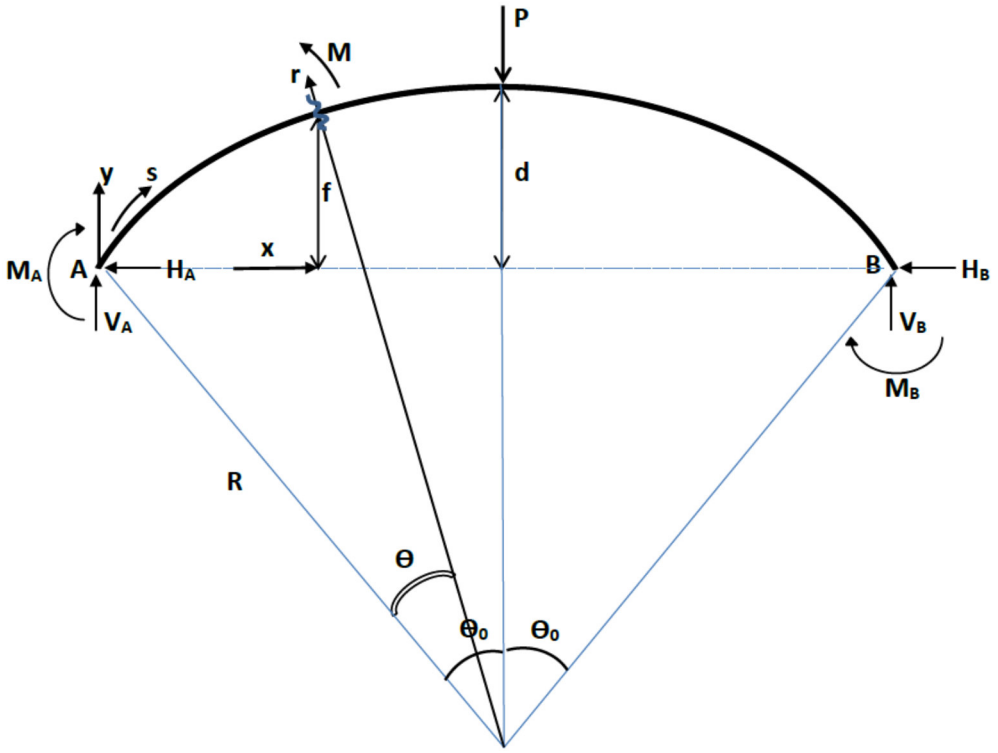

Figure 5: Parameters for analysis of a curved beam

Integrating again gives:

$$r = \frac{PR^3\left[\frac{\theta^2}{2}\sin\theta_o + \sin(\theta_o - \theta)\right]}{2EI} + C_1\theta + C_2 \qquad (13)$$

At θ = 0, r = 0,

$$C_2 = -\frac{PR^3}{2EI}\sin\theta_o$$

At θ = θ_o, dr/dθ= 0, so:

$$C_1 = \frac{PR^3[1 - \theta_o \sin\theta_o]}{2EI}$$

And

$$r = \frac{PR^3\left[\left[\frac{\theta^2}{2}\sin\theta_o + \sin(\theta_o - \theta) - \theta\theta_o \sin\theta_o + \theta - \sin\theta_o\right]\right]}{2EI} \qquad (14)$$

At $\theta = \theta_o$, the displacement is:

$$r_o = \frac{PR^3\left[[-\frac{\theta_o^2}{2}\sin\theta_o + \theta_o - \sin\theta_o]\right]}{EI} \tag{15}$$

For $\theta_o = \pi/2$,

$$r_o = \frac{PR^3\left[[-\frac{\pi^2}{8} + \frac{\pi}{2} - 1]\right]}{EI} = 0.337\frac{PR^3}{EI} \tag{16}$$

The spring constant can be defined as the ratio of load over displacement P/δ.

From equation (16), we have:

$$\frac{P}{\delta}_{curved} = \frac{EI}{0.337R^3} \tag{17}$$

For a straight beam with the same length as the curved beam ($L = \pi R$), equation (9) can be used to determine the spring constant for the straight beam:

$$\frac{P}{\delta}_{straight} = \frac{48EI}{\pi^3 R^3} = \frac{EI}{0.64R^3} \tag{18}$$

As such, for beams with similar length subjected to similar loading and boundary conditions, curved beams are stiffer than straight beams.

Equation (15) can be rewritten to evaluate the spring constant:

$$\frac{P}{\delta} = \frac{EI}{R^3(\theta_o - \sin\theta_o - \frac{\theta_o^2}{2}\sin\theta_o)} \tag{19}$$

Using equation (19), values of the spring constants for a few laminates are calculated and shown in Table 3. The variations of the spring constant with the values of *n* for laminates of type $[0_2/90_n]$ are shown in figure 6.

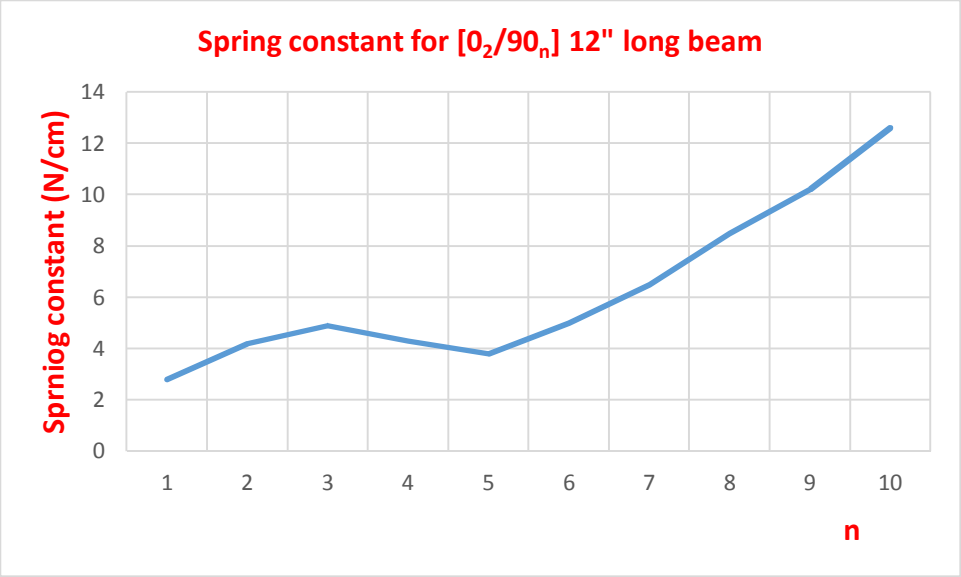

Figure 6: Variations of the spring constant with *n* for [$0_2/90_n$], 12 inch long beam.

Experimental values:

In order to validate the above calculations, two example springs were made and tested. Both springs have the lay up sequence of [$0_{16}/90_{24}$], made of carbon/epoxy, CYTEC 977-2. Both have width of 3 inch (7.62 cm). One has a length of 12 inch (30.48 cm) and the other has a length of 24 inch (60.96 cm). The two samples were made using automated fiber placement machine at Concordia Center for Composites. The samples were cured in an autoclave. The flat stacks of the layers become curved as shown in figure 7. The 0^o layers are on the convex side and the 90^o layers are on the concave side. The curvatures of the sample were measured to be 105 cm as shown in Table 3.

Strain gages were placed onto the samples, two on the convex side and one on the concave side. The two gages on the convex side are located at 4 inch (10.16 cm) from the mid length of the beam. The gage on the concave side is located at the same distance from the mid length, as the gage on the convex side. The samples were placed in an MTS machine for 3-point bending test as shown in figure 8.

Figure 7: Flat stack of layers become a curved spring (24 inch long sample)

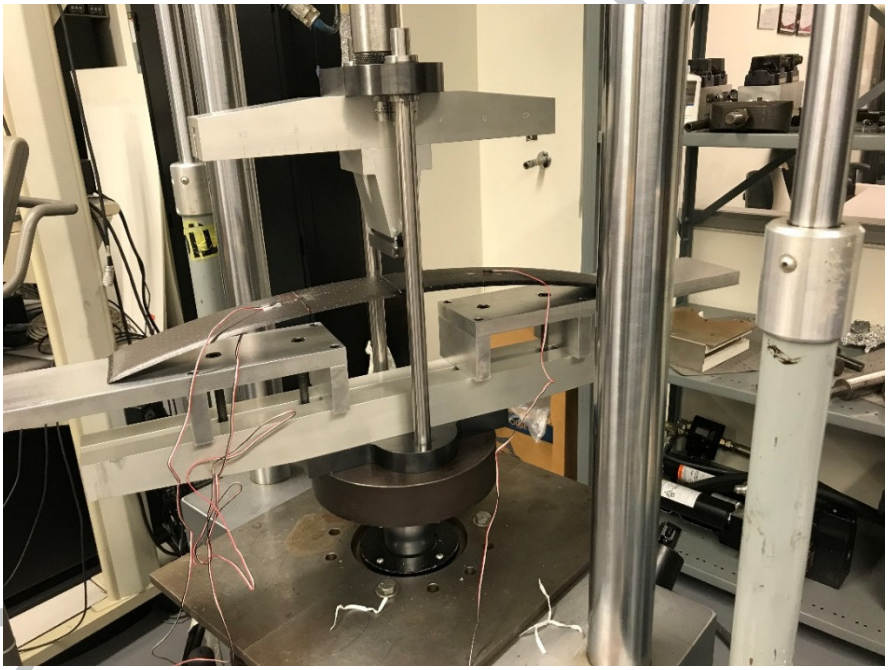

Figure 8: Sample under 3 point bending test.

In the static test, the relation between the load and deformation for two types of samples (short and long) are shown in figure 9.

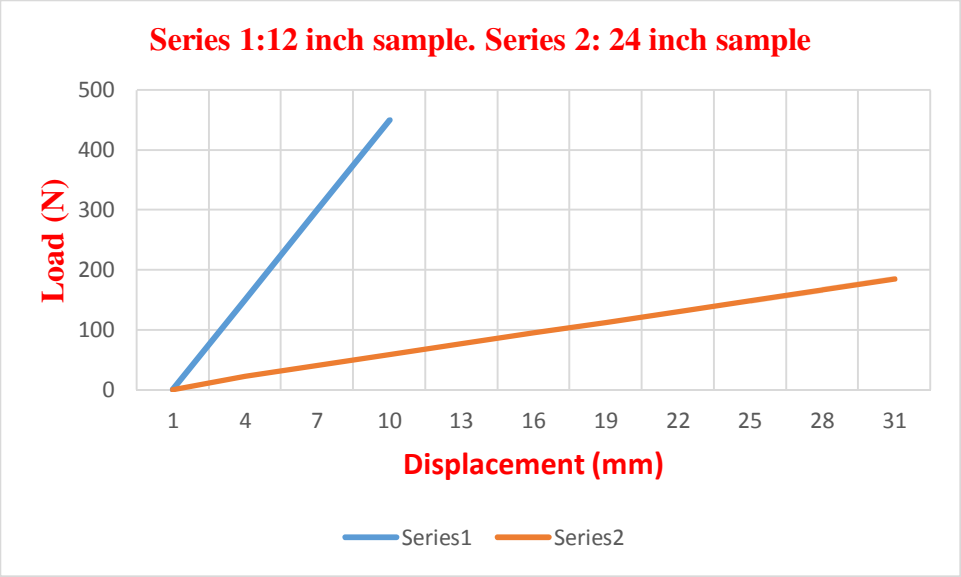

Figure 9: Load-displacement curve for long sample (24 inch long, lower curve) and short sample (12 inch long, upper curve) [12]

The spring constant (load versus displacement) is 6.0 N/cm for the long sample and about 48.6 N/cm for the short sample. In addition two more samples were made and tested. These are laminates $[0/90_7]$ and $[0_2/90_{10}]$. These spring constants are shown in Table 4. In comparison with the calculate values, reasonable agreement is obtained.

The convex side of the sample exhibits compressive strains while the concave side exhibits tensile strains. For the long sample, figure 10 shows the load versus strain curves for two strain gages placed at the same length position, but one on the convex side and the other on the concave side. It can be seen that for the same longitudinal position, the magnitude of the compressive strain on the convex side is smaller than the magnitude of the tensile strain on the concave side. At 150 N, the convex side shows -780 με whereas the concave side shows 2030 με. The load versus strain curve for the short sample (concave side) was also obtained. The short sample is stiffer than the long sample.

Strength requirement

Under loading, the configuration of the composite spring is similar to that of figure 4c. For a lay up sequence such as $[0_{16}/90_{24}]$, the upper layers are the 0^o layers and the lower layers are the 90^o layers. For durability, it is necessary that the stresses developed during loading does not exceed the strength.

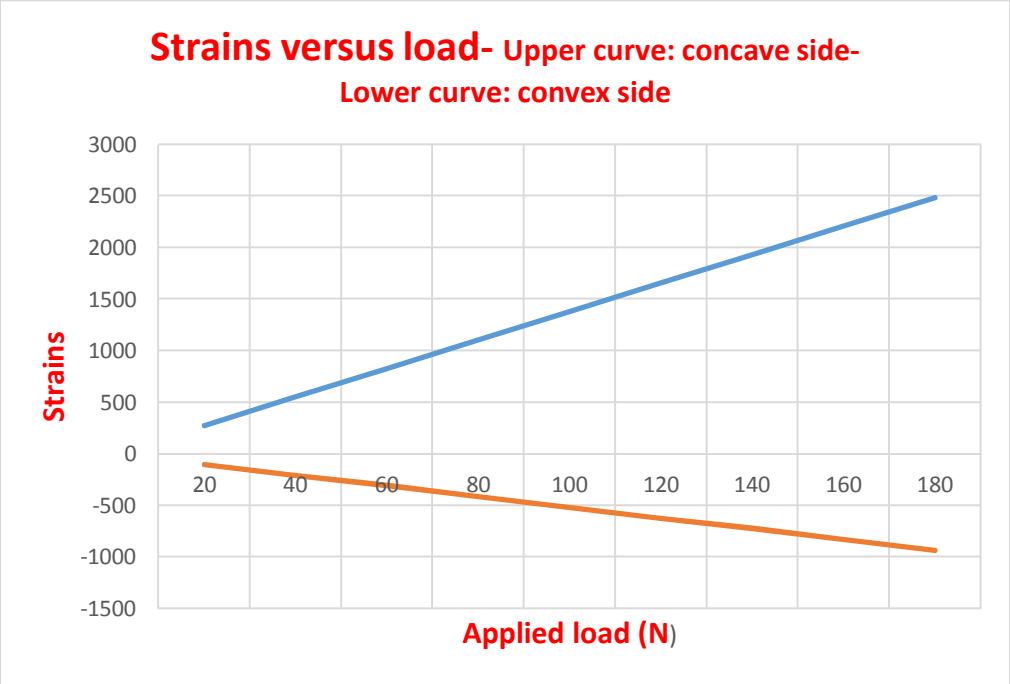

Figure 10: Load-strain in long sample (24" or 60.96 cm long) (upper curve- concave side; lower curve- convex side) [12]

The curved laminate as shown in figure 4c was subjected to residual stresses due to the difference in coefficients of thermal contraction in the different layers during cooling from the cure temperature. Analysis can be done to determine these residual stresses. Analysis can also be done to determine the stresses due to mechanical loading as in figure 4c.

Residual stresses due to cooling from cure temperature:

For a laminate subjected to a temperature gradient of ΔT, the relation between the thermal stress/moment resultants and strains and curvatures are:

$$\begin{bmatrix} N_x^T \\ N_y^T \\ N_{xy}^T \\ M_x^T \\ M_y^T \\ M_{xy}^T \end{bmatrix} = \begin{bmatrix} A_{11} & A_{12} & A_{16} & B_{11} & B_{12} & B_{16} \\ A_{12} & A_{22} & A_{26} & B_{12} & B_{22} & B_{26} \\ A_{16} & A_{26} & A_{66} & B_{16} & B_{26} & B_{66} \\ B_{11} & B_{12} & B_{16} & D_{11} & D_{12} & D_{16} \\ B_{12} & B_{22} & B_{26} & D_{12} & D_{22} & D_{26} \\ B_{16} & B_{26} & B_{66} & D_{16} & D_{26} & D_{66} \end{bmatrix} \begin{bmatrix} \varepsilon_x^o \\ \varepsilon_y^o \\ \gamma_{xy}^o \\ \kappa_x \\ \kappa_y \\ \kappa_{xy} \end{bmatrix} \quad (20)$$

For the case of cross ply laminates, it can be shown that $A_{16} = A_{26} = B_{12} = B_{16} = B_{26} = D_{16} = D_{26} = 0$. Equation (20) can be shown to consist of two decoupled equations, one containing the x and y components and the other containing the xy component. For the x and y components only, we have:

$$\begin{bmatrix} N_x^T \\ N_y^T \\ M_x^T \\ M_y^T \end{bmatrix} = \begin{bmatrix} A_{11} & A_{12} & B_{11} & 0 \\ A_{12} & A_{22} & 0 & B_{22} \\ B_{11} & 0 & D_{11} & D_{12} \\ 0 & B_{22} & D_{12} & D_{22} \end{bmatrix} \begin{bmatrix} \varepsilon_x^o \\ \varepsilon_y^o \\ \kappa_x \\ \kappa_y \end{bmatrix} \tag{21}$$

Inverting yields:

$$\begin{bmatrix} \varepsilon_x^o \\ \varepsilon_y^o \\ \kappa_x \\ \kappa_y \end{bmatrix} = \begin{bmatrix} a_{11} & a_{12} & b_{11} & b_{12} \\ a_{12} & a_{22} & b_{21} & b_{22} \\ b_{11} & b_{12} & d_{11} & d_{12} \\ b_{21} & b_{22} & d_{12} & d_{22} \end{bmatrix} \begin{bmatrix} N_x^T \\ N_y^T \\ M_x^T \\ M_y^T \end{bmatrix} \tag{22}$$

The stresses at any particular point is given as:

$$\begin{bmatrix} \sigma_x^T \\ \sigma_y^T \end{bmatrix} = \begin{bmatrix} \overline{Q_{11}} & \overline{Q_{12}} \\ \overline{Q_{12}} & \overline{Q_{22}} \end{bmatrix} \begin{bmatrix} \varepsilon_x^{oT} + z\kappa_x^{oT} - \alpha_x \Delta T \\ \varepsilon_y^{oT} + z\kappa_y^{oT} - \alpha_y \Delta T \end{bmatrix} \tag{23}$$

Where

$$\alpha_x = \alpha_1 m^2 + \alpha_2 n^2 \qquad \alpha_y = \alpha_1 n^2 + \alpha_2 m^2 \tag{24}$$

$$N_x^T = \int_{-\frac{H}{2}}^{\frac{H}{2}} (\overline{Q_{11}}\alpha_x^T + \overline{Q_{12}}\alpha_y^T + \overline{Q_{16}}\alpha_{xy}^T)\Delta T\, dz \tag{25a}$$

$$N_y^T = \int_{-\frac{H}{2}}^{\frac{H}{2}} (\overline{Q_{12}}\alpha_x^T + \overline{Q_{22}}\alpha_y^T + \overline{Q_{26}}\alpha_{xy}^T)\Delta T\, dz \tag{25b}$$

$$M_x^T = \int_{-\frac{H}{2}}^{\frac{H}{2}} (\overline{Q_{11}}\alpha_x^T + \overline{Q_{12}}\alpha_y^T + \overline{Q_{16}}\alpha_{xy}^T)\Delta T z\, dz \tag{25c}$$

$$M_y^T = \int_{-\frac{H}{2}}^{\frac{H}{2}} (\overline{Q_{12}}\alpha_x^T + \overline{Q_{22}}\alpha_y^T + \overline{Q_{26}}\alpha_{xy}^T)\Delta T z\, dz \tag{25d}$$

Stresses due to mechanical load:

Since the only mechanical load is the bending moment M_z caused by the load P, the moment resultant-strain relation can be written as:

$$\begin{bmatrix} 0 \\ 0 \\ M_z \\ 0 \end{bmatrix} = \begin{bmatrix} A_{11} & A_{12} & B_{11} & 0 \\ A_{12} & A_{22} & 0 & B_{22} \\ B_{11} & 0 & D_{11} & D_{12} \\ 0 & B_{22} & D_{12} & D_{22} \end{bmatrix} \begin{bmatrix} \varepsilon_x^o \\ \varepsilon_y^o \\ \kappa_x \\ \kappa_y \end{bmatrix} \tag{26}$$

Inverting yields:

$$\begin{bmatrix} \varepsilon_x^o \\ \varepsilon_y^o \\ \kappa_x \\ \kappa_y \end{bmatrix} = \begin{bmatrix} a_{11} & a_{12} & b_{11} & b_{12} \\ a_{12} & a_{22} & b_{21} & b_{22} \\ b_{11} & b_{12} & d_{11} & d_{12} \\ b_{21} & b_{22} & d_{12} & d_{22} \end{bmatrix} \begin{bmatrix} 0 \\ 0 \\ M_z \\ 0 \end{bmatrix} \tag{27}$$

Based on Kirchhoff assumption, the strain at any point across the thickness of the laminate can be written as:

$$\varepsilon_x = \varepsilon_x^o + zk_x = (b_{11} + d_{11}z)M_z \tag{28}$$

The neutral axis is located at:

$$z = -\frac{b_{11}}{d_{11}} \tag{29}$$

The stresses due to mechanical load at any point can be given as

$$\begin{bmatrix} \sigma_x^M \\ \sigma_y^M \end{bmatrix} = \begin{bmatrix} \overline{Q_{11}} & \overline{Q_{12}} \\ \overline{Q_{12}} & \overline{Q_{22}} \end{bmatrix} \begin{bmatrix} \varepsilon_x^{oM} + z\kappa_x^{oM} \\ \varepsilon_y^{oM} + z\kappa_y^{oM} \end{bmatrix} \tag{30}$$

Stresses due to combination of residual stresses and mechanical loads:

The stresses due to the combination of thermal residual stresses and mechanical loads can be obtained using both equations (23) and (30):

$$\begin{bmatrix} \sigma_x^C \\ \sigma_y^C \end{bmatrix} = \begin{bmatrix} \overline{Q_{11}} & \overline{Q_{12}} \\ \overline{Q_{12}} & \overline{Q_{22}} \end{bmatrix} \begin{bmatrix} \varepsilon_x^{oT} + z\kappa_x^{oT} - \alpha_x \Delta T + \varepsilon_x^{oM} + z\kappa_x^{oM} \\ \varepsilon_y^{oT} + z\kappa_y^{oT} - \alpha_y \Delta T + \varepsilon_y^{oM} + z\kappa_y^{oM} \end{bmatrix} \tag{31}$$

Example:

The particular case of the laminate $[0_{16}/90_{24}]$ will be examined here. For this, using the properties in Table 2, one has:

$$Q_{11} = 155.7\,GPa \qquad Q_{12} = 3.02\,GPa \qquad Q_{22} = 12.16\,GPa \qquad Q_{66} = 4.40\,GPa$$

For 0° layer:

$\overline{Q_{11}} = 155.7\ GPa \quad \overline{Q_{12}} = 3.02\ GPa \quad \overline{Q_{22}} = 12.16\ GPa \quad \overline{Q_{66}} = 4.40\ GPa$

$\overline{Q_{16}} = 0\ GPa \quad \overline{Q_{26}} = 0\ GPa$

For the 90° layer:

$\overline{Q_{11}} = 12.16\ GPa \quad \overline{Q_{12}} = 3.02\ GPa \quad \overline{Q_{22}} = 155.7\ GPa \quad \overline{Q_{66}} = 4.40\ GPa$

$\overline{Q_{16}} = 0\ GPa \quad \overline{Q_{26}} = 0\ GPa$

For a laminate with a stacking sequence $[0_{2m}/90_{2n}]$, (m < n), the components of the stiffness can be shown to be:

$$A_{11} = 2h[(\overline{Q_{11}})_o m + (\overline{Q_{11}})_{90} n]$$

$$A_{22} = 2h[(\overline{Q_{22}})_o m + (\overline{Q_{22}})_{90} n]$$

$$A_{12} = 2h[(\overline{Q_{12}})_o m + (\overline{Q_{12}})_{90} n] = 2h(m+n)\overline{Q_{12}} \tag{32}$$

$$B_{11} = 2mnh^2[(\overline{Q_{11}})_{90} - (\overline{Q_{11}})_o]$$

$$B_{22} = 2mnh^2[(\overline{Q_{22}})_{90} - (\overline{Q_{22}})_o] = -B_{11} \tag{33}$$

$$D_{11} = \frac{h^3}{3}[(\overline{Q_{11}})_o(6mn^2 + 2m^3) + (\overline{Q_{11}})_{90}(6m^2n + 2n^3)]$$

$$D_{22} = \frac{h^3}{3}[(\overline{Q_{22}})_o(6mn^2 + 2m^3) + (\overline{Q_{22}})_{90}(6m^2n + 2n^3)]$$

$$D_{12} = \frac{2}{3}h^3\overline{Q_{12}}(m^3 + n^3 + 3m^2n + 3mn^2) \tag{34}$$

Then, for the $[0_{16}/90_{24}]$ laminate (m = 8, n = 12)

$A_{11} = 3.48 \times 10^8$ N/m $\quad A_{12} = 0.15 \times 10^8$ N/m $\quad A_{22} = 4.91 \times 10^8$ N/m

$B_{11} = -4.31 \times 10^5$ N $\quad B_{22} = -B_{11} = 4.31 \times 10^5$ N

$D_{11} = 868$ Nm $\quad D_{22} = 880$ Nm $\quad D_{12} = 31.4$ Nm

Strains due to thermal loads:

Equation (21) becomes:

$$\begin{bmatrix} N_x^T \\ N_y^T \\ M_x^T \\ M_y^T \end{bmatrix} = \begin{bmatrix} 3.48x10^8 & 0.15x10^8 & -4.31x10^5 & 0 \\ 0.15x10^8 & 4.91x10^8 & 0 & 4.31x10^5 \\ -4.31x10^5 & 0 & 868 & 31.4 \\ 0 & 4.31x10^5 & 31.4 & 880 \end{bmatrix} \begin{bmatrix} \varepsilon_x^o \\ \varepsilon_y^o \\ \kappa_x \\ \kappa_y \end{bmatrix} \tag{35}$$

Using Mathematica to invert, one has:

$$\begin{bmatrix} \varepsilon_x^o \\ \varepsilon_y^o \\ \kappa_x \\ \kappa_y \end{bmatrix} = 10^{-3} \begin{bmatrix} 7.5x10^{-6} & -1.97x10^{-7} & 3.7x10^{-3} & -3.63x10^{-5} \\ -1.97x10^{-7} & 3.6x10^{-6} & -3.42x10^{-5} & -1.76x10^{-3} \\ 3.7x10^{-3} & -3.42x10^{-5} & 3.01 & -9.0x10^{-2} \\ -3.63x10^{-5} & -1.76x10^{-3} & -9.0x10^{-2} & 2.0 \end{bmatrix} \begin{bmatrix} N_x^T \\ N_y^T \\ M_x^T \\ M_y^T \end{bmatrix} \tag{36}$$

The thermal stress resultants and moment resultants are calculated using equations (25) to be:

$$N_x^T = 8.22x10^6 h\Delta T \quad N_y^T = 6.42x10^6 h\Delta T$$
$$M_x^T = 8.64x10^7 \frac{h^2}{2}\Delta T \quad M_y^T = -8.64x10^7 \frac{h^2}{2}\Delta T \tag{37}$$

Using the value of h= 0.125 mm and ΔT = 20-177 = -157 ºC into equation (37) gives the following values:

$$N_x^T = -161,318\ N/m \quad N_y^T = -126,008\ N/m$$
$$M_x^T = -106\ N \quad M_y^T = 106\ N \tag{38}$$

Substituting into equation (36) gives

$$\varepsilon_x^o = -1.36x10^{-3}$$
$$k_x = -0.921 \tag{39}$$

The strain at any point across the thickness of the laminate is given as:

$$\varepsilon_x = \varepsilon_x^o + z\kappa_x \ or$$
$$\varepsilon_x = -1.36x10^{-3} - 0.921z \tag{40}$$

The neutral surface is where the strain is equal to 0:

$$z = \frac{1.36x10^{-3}}{-0.921} = -1.472mm$$

This is located about 12 layers above the mid plane, and is within that 0º layers. Location of the neutral surface is as shown in figure 11.

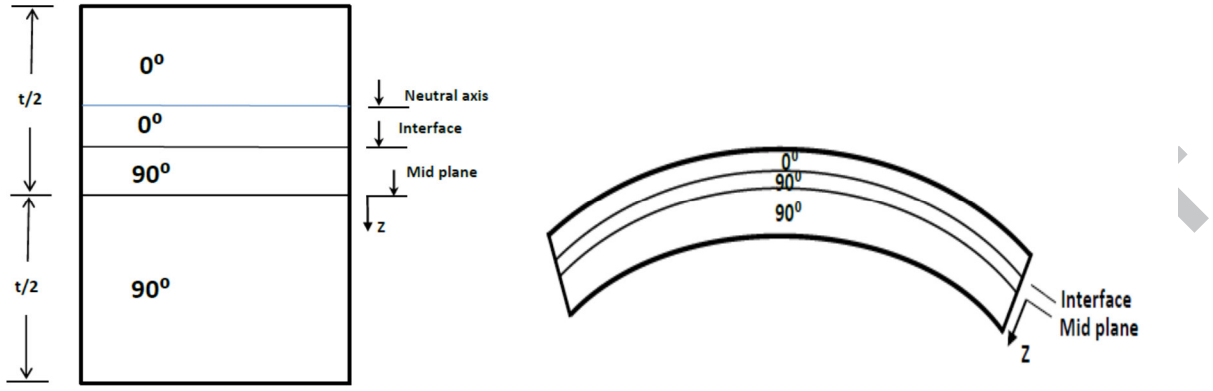

Figure 11: Locations of mid plane, neutral surface and interface

Using equation (40), the strains at different critical locations are:

Position	**Strains (με)**
Concave surface (90° layers) (z = 2.5 mm)	-3660
Convex surface (0° layers) (z = -2.5 mm)	947
Interface between 90° and 0° layers, z=-0.5mm	-946

It can be seen that all of the 90° layers are under compressive strains, while some of the 0° layers (about 10 layers) are under compressive strains, while the rest of the 0° layers (about 6 layers) are under tensile strain.

Strains due to mechanical load:

Equation (36) can be used to write the strain-stress resultant for the case of mechanical load as:

$$\begin{bmatrix} \varepsilon_x^o \\ \varepsilon_y^o \\ \kappa_x \\ \kappa_y \end{bmatrix} = 10^{-3} \begin{bmatrix} 7.5x10^{-6} & -1.97x10^{-7} & 3.7x10^{-3} & -3.63x10^{-5} \\ -1.97x10^{-7} & 3.6x10^{-6} & -3.42x10^{-5} & -1.76x10^{-3} \\ 3.7x10^{-3} & -3.42x10^{-5} & 3.01 & -9.0x10^{-2} \\ -3.63x10^{-5} & -1.76x10^{-3} & -9.0x10^{-2} & 2.0 \end{bmatrix} \begin{bmatrix} 0 \\ 0 \\ M_z \\ 0 \end{bmatrix}$$

The strain at any point can be written as:

$$\varepsilon_x = (3.7x10^{-6} + 0.003\,z)M_z \tag{41}$$

Combining equations (40) and (41), the combined strains due to residual thermal stresses and applied mechanical load is:

$$\varepsilon_x = -1.36x10^{-3} + 3.7x10^{-6}M_z + (-0.921 + 0.003M_z)z \tag{42}$$

The neutral axis corresponds to when the strain is zero, given by:

$$z_n = \frac{1.36x10^{-3} - 3.7x10^{-6} M_z}{-0.921 + 0.003M_z} \quad (43)$$

Based on figure 4c, the bending moment at a section of the beam depends on the location of the beam. As such, the neutral axis would vary along the length of the beam. From the experimental result, the load P varies from 0 to 200 N, and half length of the beam is 6 inch (about 15 cm). As such, the range for the bending moment is from 0 to 15 N.m. The influence of the bending moment on the strength of the laminate can be examined by examining the strains at the bottom of the laminate. At the bottom of the laminate (90^o layers), z = 2.5 mm, and from (42), the strain is -3500 με. This shows that the strains on the 90^o layers are always compressive. The 24 inch (60.96 cm) long sample was subjected to fatigue test under three-point bending with maximum displacement of 2.4 mm and minimum displacement of 0.24 mm for 175,000 cycles. The spring constant of the laminate did not change after the fatigue test.

Conclusion: It was shown that it is possible to make composite springs with practical stiffnesses and strengths comparable with composite springs that are currently used, using the method of 4D printing of composites. The method of 4D printing of composites allows the manufacturing of curved structures without the need for curved molds.

Acknowledgement: The financial support from the Natural Sciences and Engineering Research Council of Canada is appreciated. The supports for the manufacturing of the samples by Mrrs Jeff Simpson, Daniel Rosca, and Duc Hoang are appreciated.

References:

1. https://www.exporterindia.com/shandon/fully/cabin-leaf-springs-china-431207.htm.
2. https://www.ottobockus.com/sports/solution-overview/3s80-and-sprinter-foot.
3. Shokrieh R.D., "Analysis and optimization of composite leaf spring", Composite Structures, No. 60, 2003, pp. 317-325.
4. Beardmore J.C., "The potential for composites in structural automotive applications", Composites Science and Technology, No. 26, 1986, pp. 251-281.
5. Morris C.J., "Composite integrated rear suspension", Composite structures, No. 5, 1986, pp. 233-242.
6. Daugherty R.L., "Composite leaf springs in heavy truck applications", in Composite Materials, Proceedings of the US-Japan conference, Tokyo, 1981.
7. Yu W.J., and Kim H.C., "Double tapered FRP beam for automotive suspension leaf spring", Composite structures, No. 9, 1988, pp. 279-300.
8. Tibbits S., "The emergence of 4D printing", TED conference, 2013.
9. Farhang Momeni, Seyed M. Mehdi, Hasani N., Xun Liu, and Jun Ni, "A review of 4D printing", Materials and Design, 122, 2017, pp. 42-79.
10. Hoa Suong Van, "Factors affecting the properties of composites made by 4D printing (moldless composite manufacturing)", Advanced Manufacturing: Polymer & Composites Science, Vol. 3, No. 3, 2017, pp. 101-109.
11. Hyer M.W., "Stress analysis of fiber-reinforced composite materials", Destech Publications, 2009.

12. M. S. Gill,"Development and fabrication of carbon/epoxy composite leaf springs using 4D printing", Project report (ENGR 6991), Concordia University, 2018.